Dynamics, Structure and Function of Biological Macromolecules
O. Jardetzky and M.D. Finucane (Eds.)
IOS Press, 2001

STRUCTURES OF HUMAN PEPTIDE HORMONES IN SOLUTION

Ute Marx[1,2], Knut Adermann[2], Axel Schulz[2], Markus Meyer[2], Wolf-Georg Forssmann[2], and Paul Rösch[1]

[1]*Dept. of Biopolymers, U. of Bayreuth, D95440 Bayreuth, Germany*
[2]*Institute for Peptide Research, D30625 Hannover, Germany*

ABSTRACT. Human peptide hormones are components of various regulation mechanisms. Parathyroid hormone (PTH), for example, is involved in calcium homeostasis in blood and, additionally, plays a crucial role in bone metabolism. Uroguanylin is part of the intestinal epithelial electrolyte regulation machinery acting via the guanylyl cyclase pathway.
Structure determination of peptide hormones is an important step to correlate structure and function, to understand endocrine diseases on a molecular level, and to design therapeutics mimicking the peptide structure.

1. HUMAN PARATHYROID HORMONE

1.1 Introduction

The complete human PTH (hPTH) consists of 84 amino acids. All known endocrine function is located in the NH_2-terminal 34 amino acids and is transduced *via* the adenylate cyclase and the phosphatidyl inositol pathways. The fragment found in human blood is hPTH(1-37) (Hock *et al.*, 1997). Earlier studies claimed that hPTH(1-34) formed stable elements of regular secondary structure only in the presence of crowding reagents such as trifluoroethanol and does not show tertiary contacts. We found, however, that both hPTH(1-37) and hPTH(1-34) consist of two helices connected by a flexible hinge and a definded loop region which is stabilized by tertiary, hydrophobic interaction between Leu15 and Trp23 in aqueous buffer solution under near physiological conditions. It is well known that truncation of the first two amino acids leads to a complete loss of *in vivo* normocalcemic function (Coleman *et al.*, 1994; Marx *et al.*, 1998a). To correlate loss of the calcium level regulatory activity after stepwise NH_2-terminal truncation and the solution structures, we determined the conformations of hPTH(1-37), hPTH(2-37), hPTH(3-37), and hPTH(4-37) in aqueous buffer solution under near physiological conditions by two-dimensional (2D) NMR spectroscopy and restrained molecular dynamics calculations. We found that the loss of calcium regulatory activity is accompanied by weakening and finally by the complete loss of the short NH_2-terminal helix. As a first step in the design of a synthetic drug we could show that the NH_2-terminal helix can be restored by acetylation or succinylation of the NH_2-terminus of the shortened peptide.

1.2. Biological Activity

The *in vivo* biological activity of hPTH(1-37), hPTH(2-37), hPTH(3-37), and hPTH(4-37) relative to hPTH(1-34) as a standard was tested using Parsons' Chicken

Assay (Parsons *et al.*, 1973). Pure solvent without PTH served as a control. The variation of the calcium level in blood was used as indicator for PTH activity. After subtraction of the control value, data are expressed as percentage of the hPTH(1-34) value and are plotted as the mean from eight separate experiments (Fig. 1).

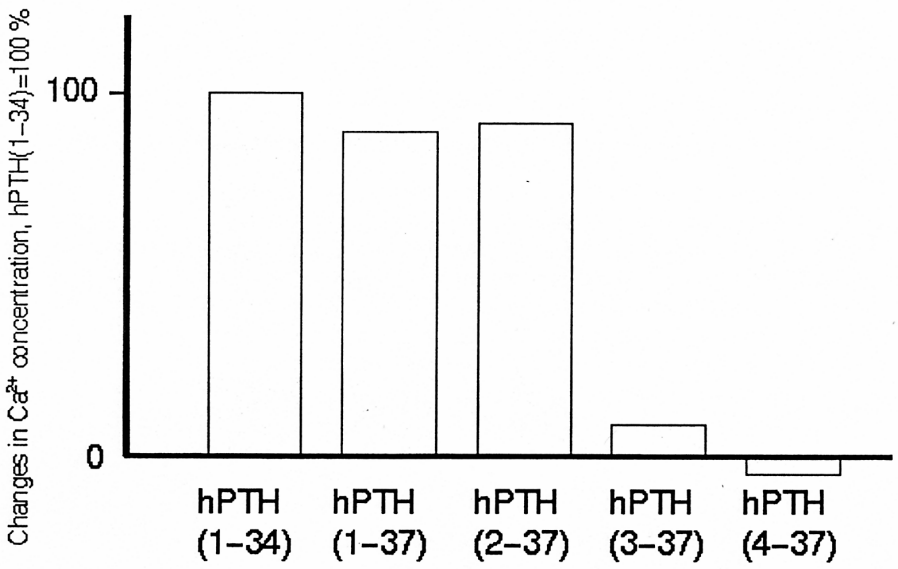

Figure 1. *In vivo* activity test of hPTH(1-37), hPTH(2-37), hPTH(3-37), and hPTH(4-37) relative to hPTH(1-34) as a standard using Parsons' Chicken Assay (Parson *et al.*, 1973; Marx *et al.*, 1998a).

The biological activities of hPTH(1-34), hPTH(1-37), and hPTH(2-37) are virtually identical in the *in vivo* activity tests of calcium homeostasis in blood. Fragment hPTH(3-37) shows less than 10 % of this activity, and hPTH(4-37) is inactive (Fig. 1). The same results are found for fragments extending to amino acid 34 (Coleman *et al.*, 1994). But amino-terminally shortened peptides have strong *in vivo* antagonistic properties, which means that the receptor binding ability remains unimpaired (Segre *et al.*, 1979; Chorev & Rosenblatt, 1994; Coleman *et al.*, 1994).

1.3. Structures of Different hPTH Fragments

Homonuclear two dimensional NMR spectra - DQF-COSY spectra, Clean-TOCSY spectra with mixing times of 80 ms, and NOESY spectra with mixing times of 200 ms - were obtained on a Bruker DMX600 spectrometer at 298 K and were used for the sequence-specific assignment of the spin systems and the evaluation of the NOESY distance restraints for structure calculation of the different PTH fragments. For hPTH(4-37) an additional set of spectra was measured at 288 K to

resolve frequency degeneration. The measurements were carried out in 50 mM phosphate buffer with 270 mM sodium chloride.

Only NOEs visible in the NOESY spectra at 298 K were used in the structure calculations. Distance geometry (DG) and molecular dynamics (MD) calculations were performed with the XPLOR 3.1 program package (Brünger *et al.*, 1993). For hPTH(1-37), 520 NOESY cross peaks were used for structure calculation, of which 183 were interresidual cross peaks. The number of nontrivial interresidual NOESY cross peaks used for structure calculation was 171 for hPTH(2-37), 210 for hPTH(3-37), and 159 for hPTH(4-37). These cross peaks were divided into three groups according to their relative intensities: strong, 0.2 to 0.3 nm, medium, 0.2 to 0.4 nm, and weak, 0.2 to 0.5 nm. 0.05 nm was added to the upper distance limit for distances involving unresolved methyl or methylene proton resonances. The structure calculations followed standard procedures employing a hybrid DG-restrained MD approach with simulated annealing (SA) refinement and subsequent energy minimization. For each fragment 30 structures were calculated. 10 structures for every fragment were selected on the criteria of having the smallest number of NOE violations over 0.05 nm and the lowest overall energy.

1.3.1. The Structure of hPTH(1-37)

Distinctive structural elements of biologically active hPTH(1-37) determined under near physiological conditions are; a short NH_2-terminal helix between Ile5 and Asn10 followed by a flexible hinge around Gly12/Lys13, a longer COOH-terminal helix from Ser17 to at least Leu28, and a defined loop region from His14 to Ser17, stabilized by hydrophobic interactions between Leu15 and Trp23 (Marx *et al.*, 1995; Fig. 2).

The loop region from His14 to Ser17 and the following COOH-terminal helix comprise the major part of the receptor binding region that is known to reside within His14 to Phe34 (Caulfield *et al.*, 1990). The structured amino-terminus (helix between Ile5 to Asn10) correlates with the activation domain responsible for the regulation of the calcium level in blood (Chorev & Rosenblatt, 1994).

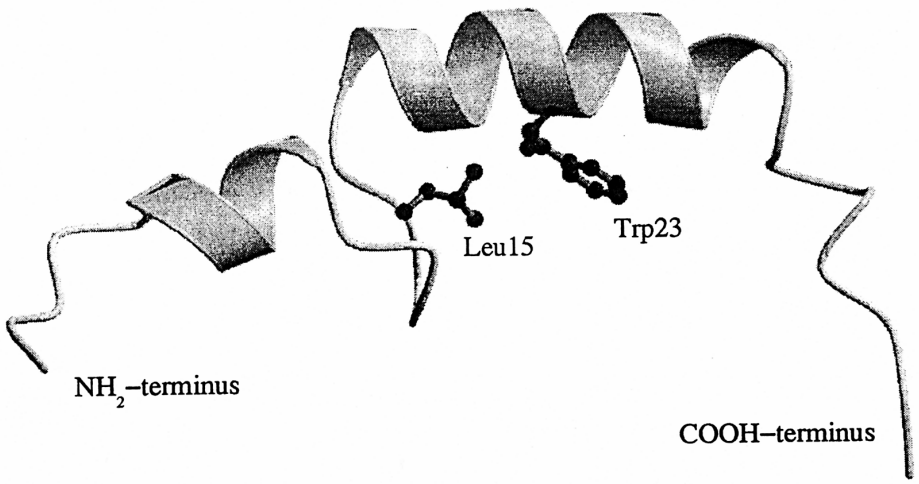

Figure 2. NMR solution structure of hPTH(1-37) in aqueous buffer solution under near physiological conditions (Marx *et al.*, 1995).

Unrestrained molecular dynamics simulations in a box of water molecules indicated that this structure is stable on a 200 ps time scale with respect to the helices and the hydrophobic interactions (Marx *et al.*, 1995). However, NMR data (chemical shift index and sequential and medium range NOE intensities) and far UV-CD measurements indicate the existence of an equilibrium between an α-helix and a more extended conformation, most probably a 3_{10}-helical structure, for both helices. The COOH-terminal helix is more rigid than the NH_2-terminal one.

1.3.2. The Structures of NH_2-Terminally Truncated hPTH Fragments

1.3.2.1. Chemical shifts and medium range NOEs

In order to allow an initial mutual comparison of the truncated fragments and hPTH(1-37), we used the chemical shift data available from our experiments to perform a secondary structure estimation based on the chemical shift index (Wishart *et al.*, 1992; 1995). This procedure depends on a direct correlation between the chemical shifts of Cα-proton resonances of consecutive amino acids and the local secondary structure (Wishart *et al.*, 1991) (Fig. 3).

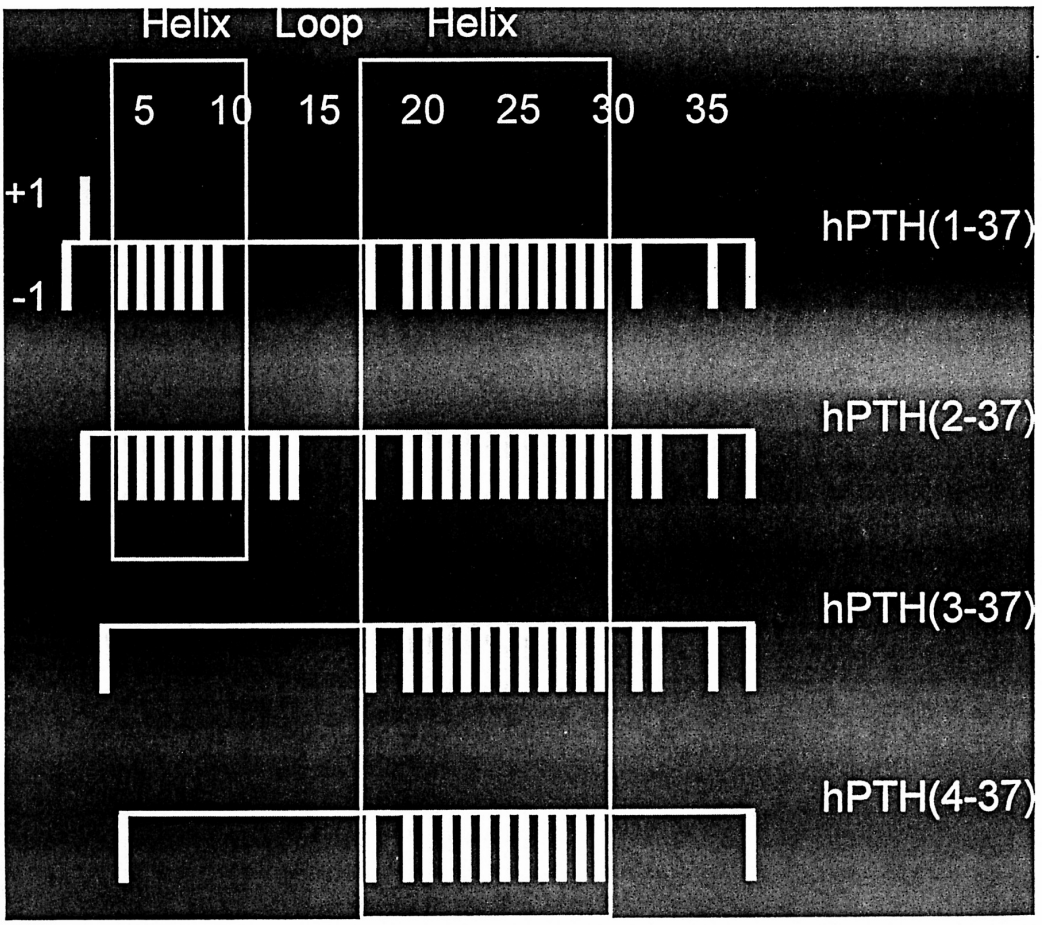

Figure 3. Chemical shift index of Cα-proton chemical shifts of hPTH(1-37), hPTH(2-37), hPTH(3-37) and hPTH(4-37) according to Wishart *et al.* (1992) using the "random coil" values of Wishart *et al.* (1995).

For hPTH(1-37) and hPTH(2-37), the chemical shifts of Cα-proton resonances suggest two helical regions extending from Ser17 to at least Gln29 and around Glu4 to His9. In contrast, no indication of an NH_2-terminal helix is found for hPTH(3-37) and hPTH(4-37), although the helical region in the COOH-terminal part can clearly be derived. No other elements of regular secondary structure were in evidence using this procedure (Fig. 3).

These results are confirmed by the medium range NOESY cross peaks observed for the various hPTH fragments from the 200 ms NOESY spectra at 298 K (Fig. 4). The $d_{\alpha N}(i,i+3)$ and $d_{\alpha\beta}(i,i+3)$ NOESY cross peaks fully corroborate the existence of two helical regions for hPTH(1-37) and hPTH(2-37). Indications for an NH_2-terminal helix for hPTH(3-37) are weak and are entirely missing for hPTH(4-37). In contrast, clear evidence of the COOH-terminal helix is found for all fragments from Ser17 to Phe34 or His32 (Fig. 4).

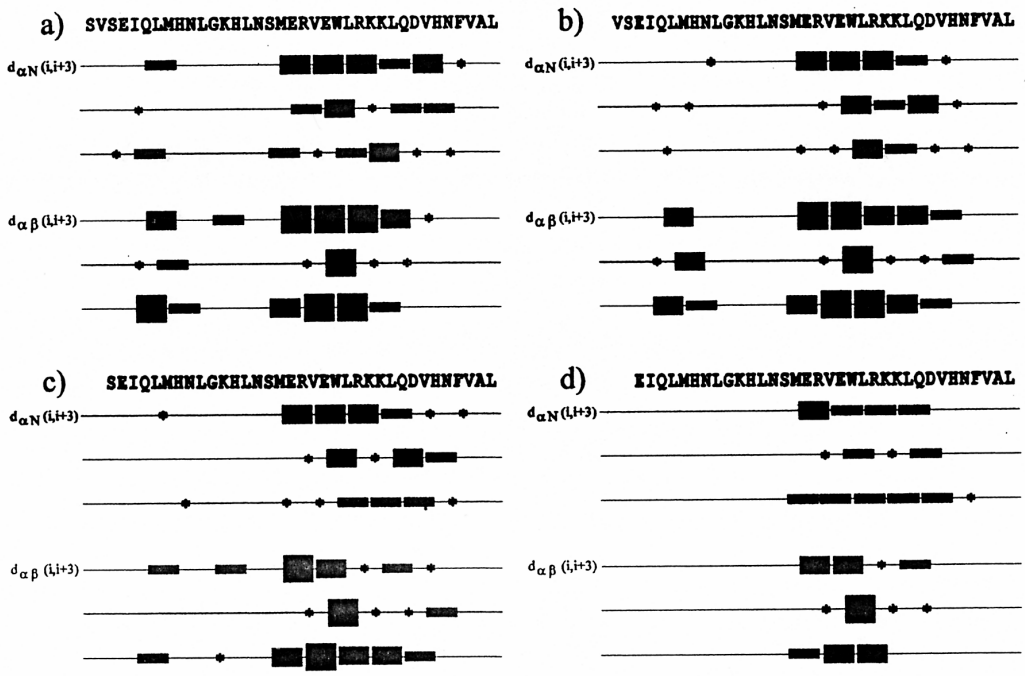

Figure 4. Patterns of (i,i+3) NOESY cross peaks (typical of helices) *versus* peptide sequence. The thickness of the bars corresponds to the relative intensities of the NOESY cross peaks. An asterisk indicates that the NOE could not be unambiguously assigned because of degenerate frequency. a) hPTH(1-37), b) hPTH(2-37), c) hPTH(3-37), d) hPTH(4-37).

In addition, all fragments show several long range NOEs between Leu15 and Trp23, indicating spatial proximity between these two residues, probably due to hydrophobic interactions. The observed NOEs are responsible for a clear restriction of the conformational space of the calculated structures and lead to a defined loop region around His14 to Ser17. Furthermore, due to the ring current field of the spatial neighbouring aromatic ring system of Trp23, the δ-proton resonances of Leu15 are

shifted upfield in comparison to the analogous resonances of other leucines for all four fragments (Marx *et al.*, 1998a).

1.3.2.2. Structure calculations

159 to 210 interresidual NOEs per fragment were collected from 200 ms NOESY spectra at 298 K and used for restrained MD calculations.

Each of the four fragments exhibit the COOH-terminal helix extending from Met18 to at least Leu28. An NH_2-terminal helix between Ile5 and Asn10 exists in hPTH(1-37). In hPTH(2-37), five structures show an NH_2-terminal α-helix around Leu7, the others show turns or 3_{10}-helices in this region. None of the ten calculated minimal energy structures of hPTH(3-37) displays an NH_2-terminal α-helix, only two structures exhibit a 3_{10}-helix from Glu4 to Gln6. No structure of hPTH(4-37) shows an NH_2-terminal helix, and only in one case a turn is found in this region. The extent of the COOH-terminal helix of hPTH(4-37) is virtually identical to that of the corresponding helix in the other fragments. The loss of the NH_2-terminal helix after truncation of the first two amino acids is thus corroborated by the structure calculations (Marx *et al.*, 1998a).

The two biologically inactive fragments hPTH(3-37) and hPTH(4-37) show the same loop region around His14 to Ser17 and the following COOH-terminal helix from Met18 to at least Leu28 as the fragments hPTH(1-37) and hPTH(2-37). This well defined region from His14 to at least Leu28 is part of the postulated receptor binding site from His14 to Phe34 (Caulfield *et al.*, 1990; Lopez-Hilker *et al.*, 1992). Indeed, NH_2-terminally truncated biologically inactive hPTH fragments such as PTH(3-34) have complete receptor binding ability (Segre *et al.*, 1979; Chorev & Rosenblatt, 1994).

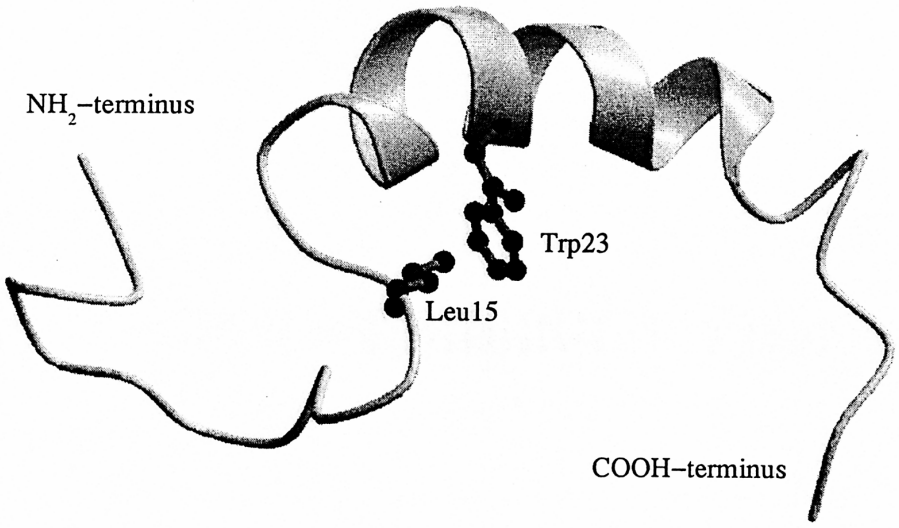

Figure 5. NMR solution structure of hPTH(3-37) in aqueous buffer solution under near physiological conditions.

1.3.2.3. Conclusions

In vivo normocalcemic function of hPTH(1-37) is lost on deletion of the two NH_2-terminal amino acids, but receptor binding ability remains unimpaired (Coleman *et al.*, 1994; Chorev & Rosenblatt, 1994). The NH_2-terminal helix is lost on NH_2-terminal truncation, but the loop region and the COOH-terminal helix remain intact. Both the loop and the helix form the major part of the receptor binding site that is known to reside within His14 to Phe34 (Caulfield *et al.*, 1990; Lopez-Hilker *et al.*, 1992). As the NH_2-terminal helix is only present in the *in vivo* bioactive fragments hPTH(1-37) and hPTH(2-37), but not in the inactive fragments hPTH(3-37) and hPTH(4-37), this may indicate that the NH_2-terminal helix is correlated with the *in vivo* bioactivity of the PTH fragments with respect to the calcium level in blood (Marx *et al.*, 1998a).

1.4. Restoration of the NH_2-Terminal Helix

To decide whether or not the *in vivo* activity is determined on a structural level by the NH_2-terminal helix or depends on a direct functional role of the first two amino acids, we tried to reconstruct this helix. It is well known that interactions between charged groups close to the end of a helix and the helix dipoles are an important determinant of α-helix stability (Fairman *et al.*, 1989). For example, free α-NH_3^+-groups are helix-destabilizing as they result in unfavorable electrostatic interactions of the positive charge with the positive pole of the helix dipole. NH_2-terminal truncations bring this positive charge closer to the helix and result in a destabilisation and finally in a loss of the NH_2-terminal helix for hPTH(3-37) and hPTH(4-37). Removal of the charge from a free α-NH_3^+-group by addition of an acetyl blocking group or conversion of the positive charge to a negative one by addition of a succinyl blocking group should therefore result in a helix-stabilizing effect. We therefore synthesized two amino-terminally altered hPTH(4-37) fragments, namely acetyl-hPTH(4-37) and succinyl-hPTH(4-37).

NMR analysis and structure calculations of acetyl-hPTH(4-37) and succinyl-hPTH(4-37) were carried out as described for the NH_2-terminally truncated hPTH fragments.

The chemical shifts of the Cα-protons as well as the sequential and medium range NOEs indicate that the NH_2-terminal helix could be restored by changing the NH_2-terminal charge. Direct comparison of the Cα-proton chemical shifts of both stabilized fragments with those of hPTH(4-37) and hPTH(1-37) indicate that both modifications restore the NH_2-terminal helical structure, with the succinyl group stabilizing the helix more efficiently. For both fragments medium range helical NOEs confirm the presence of the COOH-terminal helix from Ser17 to at least Leu28. The long range interactions between Leu15 and Trp 23 which define the loop region from His14 to Ser17 are also found. In contrast to hPTH(3-37) and hPTH(4-37), (i,i+3) helical NOEs occur in the NH_2-terminal region of the peptides, with more intensive ones for succinyl-hPTH(4-37).

Both modified fragments show the NH_2-terminal helix (Fig. 6), the loop and the COOH-terminal helix, the latter two which are identical to all other studied PTH fragments. Thus one may expect that the NH_2-terminally stabilized hPTH-fragments acetyl-hPTH(4-37) and succinyl-hPTH(4-37) have receptor binding ability. *In vivo* activity assays are expected to reveal whether the existence of an NH_2-terminal helix is indeed crucial for the regulation of the calcium level in blood.

2. UROGUANYLIN

2.1. Introduction

The target protein of the peptide hormone uroguanylin is the intestinal guanylyl cyclase C (GC-C), an *E. coli* heat-stable enterotoxin receptor, which stimulates chloride secretion *via* cGMP as a second messenger. The 16 amino acid peptide hormone contains two disulfide bridges in a 1-3/2-4 arrangement (Fig. 7),

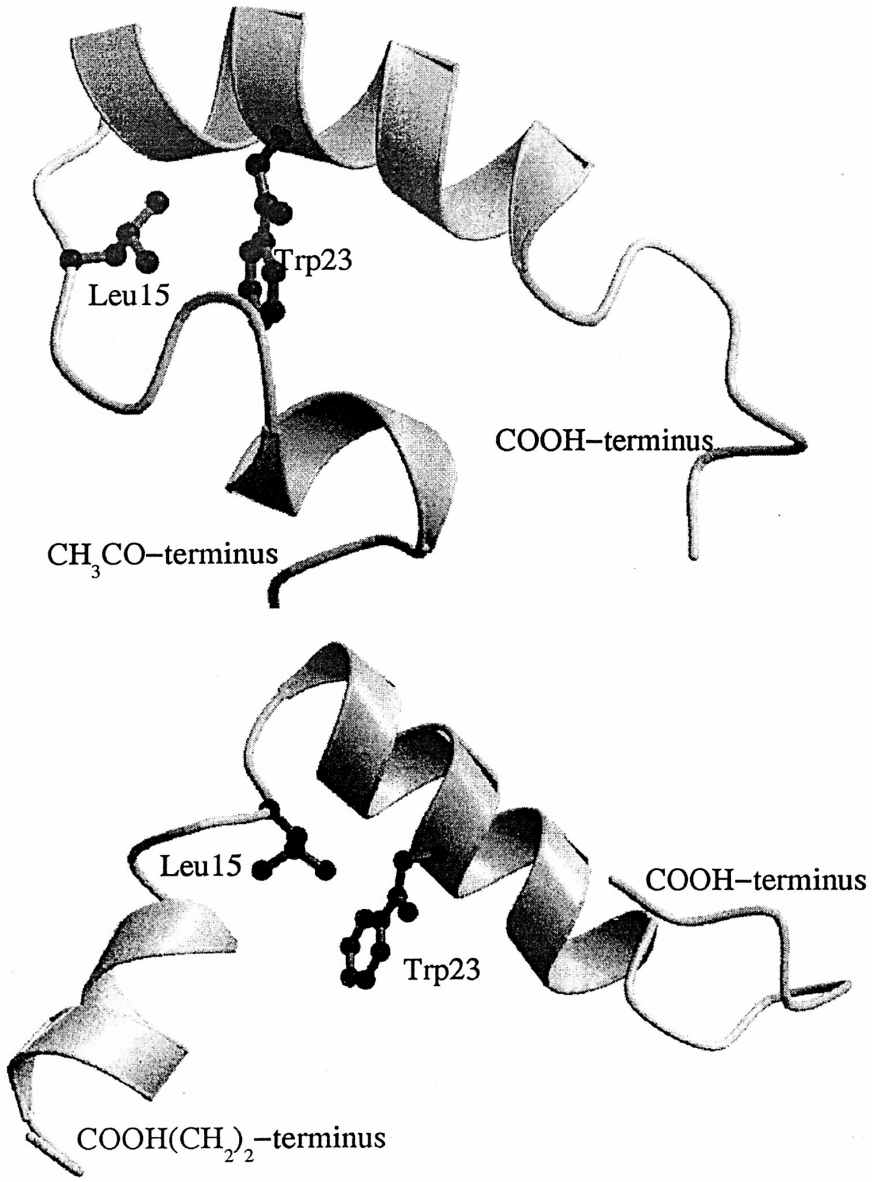

Figure 6. NMR solution structures of acetyl-hPTH(4-37) (upper) and succinyl-hPTH(4-37) in aqueous buffer solution under near physiological conditions.

giving rise to two topologically different isomers, only one of which induces intracellular cGMP elevation. To obtain an unambiguous structure/function relationship of the isomers, which are stable at 11 °C, we determined the solution structures of the separated uroguanylin isoforms using 2D NMR spectroscopy and molecular dynamics methods (Marx *et al.*, 1998b). Both isomers adopt well-defined structures that correspond to those of the isomers of the related peptide guanylin (Skelton *et al.*, 1994). The structure of the GC-C activating uroguanylin isomer A closely resembles the structure of the agonistic *E. coli* heat-stable enterotoxin. Interconversion dynamics between the two isomers as studied by HPLC and NMR under various conditions showed that the interconversion rate of uroguanylin is significantly retarded compared to the interconversion rate of the isomers of the strongly related peptide
guanylin. The conformational exchange is most likely under the steric control of the carboxy-terminal leucine as this residue is missing in guanylin and a synthetic guanylin extended by a COOH-terminal leucine shows significantly stabilized topological isomers.

2.2. Homologies and Related Peptides

Uroguanylin, of which different molecular forms were identified in urine, blood and the intestine is closely related to guanylin at the primary structure level (Fig. 7). Both peptides are characterized by two disulfide bonds in relative positions 1-3 and 2-4 which are crucial for biological activity (Forte and Currie, 1995; Klodt *et al.*, 1997). The disulfides are located in a short sequence of only 12 amino acid residues. This structural element results in the existence of two topological isoforms of each peptide (Skelton *et al.*, 1994; Klodt *et al.*, 1997; Marx *et al.*, 1998b; Schulz *et al.*, 1998). The *E. coli* heat-stable enterotoxin ST with an equivalent pattern of disulfides has an additional, third disulfide bridge which may enhance its conformational rigidity (Gariepy *et al.*, 1987). In binding assays, guanylin and uroguanylin compete with radioactively labeled *E. coli* ST for binding to their

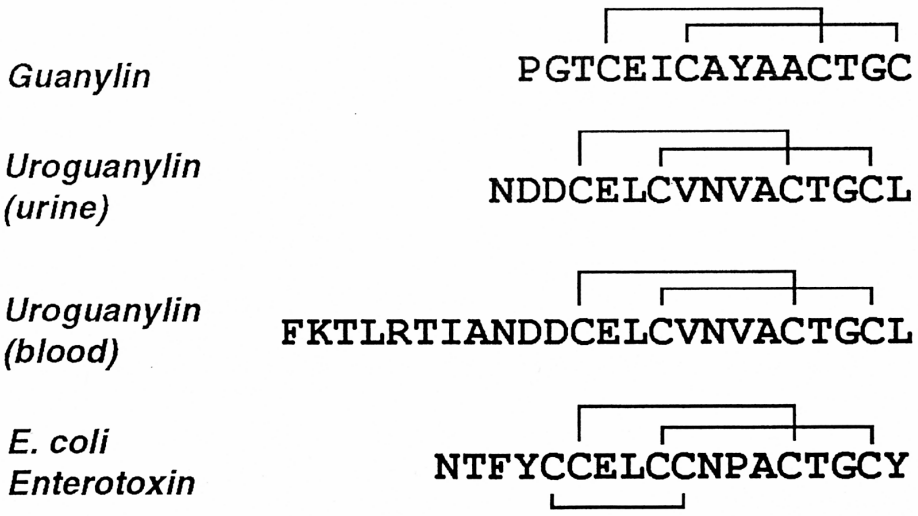

Figure 7. Amino acid sequences and disulfide pattern of GC-C activating peptides. The primary structures of human uroguanylin-16 isolated from urine, uroguanylin-24 isolated from human blood filtrate, human guanylin, and *E. coli* heat-stable enterotoxin ST are shown.

common receptor GC-C, but the endogeneous peptides are less potent activators of GC-C than ST (Carpick and Gariepy, 1993).

A unique structural feature of guanylin and uroguanylin as demonstrated by NMR and synthesis studies is the formation of topological stereoisomers (Skelton *et al.*, 1994; Chino *et al.*, 1996; Klodt *et al.*, 1997; Marx *et al.*, 1998b). These isomers exhibit the same cysteine connectivity, but are conformationally distinct molecules. The guanylin isoforms, however, are in a fast interconversion equilibrium which prevents the characterization of the isolated molecular species by NMR (Klodt *et al.*, 1997).

2.3. Structure Calculation of the Separated Uroguanylin-16 Isomers

To establish an unambiguous structure/activity relationship of uroguanylin, we combined NMR-spectroscopic structure determination of the two separated isomers of human uroguanylin with the GC-C activating potential of the single isomers. The GC-C activating compound that is also eluting earlier in HPLC analysis is referred to as isomer A.

Two dimensional NMR spectra were obtained on AMX600 and AMX400 spectrometers at 11 °C. The measurements were carried out in aqueous solution. For the sequence-specific assignment of spin systems and the evaluation of the NOESY distance constraints for the different peptides, data from the following 600 MHz spectra were employed: DQF-COSY spectra, Clean-TOCSY spectra with mixing times of 80 ms, NOESY spectra with mixing times of 200 ms, and JR-NOESY spectra with mixing times of 200 ms.

With very little resonance overlap, the sequence-specific assignment of each species could be performed by standard methods. For both isoforms the chemical shift values of residues Cys7 to Leu16 comprising the Cys-rich region are clearly different (up to 1 ppm for the amide protons between the two isoforms), indicating that the backbone folds in these regions are different.

84 and 69 distance restraints from the 200 ms NOESY spectra at 11°C together with 8 and 6 dihedral angle restraints were used for the structure calculation of uroguanylin-16 isomer A and B, respectively. A modified *ab initio* simulated annealing protocol was used with explicit inclusion of disulfide bonds. None of the 10 selected structures shows NOE violations of more than 0.03 nm, and no structure has angle violations of more than 5°. Although only a few nonsequential NOEs were assigned, and no typical NOEs and no consecutive $^{3}J_{NH\alpha H}$ coupling constants indicative of any regular secondary structure element were found, the NMR-data were sufficient to define well structured global folds for both isoforms (Fig. 8).

The well-defined global fold of the region from Cys4 to Cys15 is reflected by the low backbone root-mean square deviation (RMSD) of 0.075 nm for the A form and 0.063 nm for the B form. The structures of the isomers A and B of uroguanylin are significantly different with a backbone RMSD of 0.46 nm between the average structures of the A and B forms between residues Cys4 and Cys15.

The structure of the A form can be described as a right-handed spiral which is stabilized by the disulfide bonds Cys4-Cys12 and Cys7-Cys15. The structure of the 13 carboxy-terminal amino acids of the B form can be depicted as a distorted left-handed spiral (Fig.8 B, C). As for the A form, the three amino-terminal amino acids are unstructured and no regular secondary structure elements except reverse turns were found for the ten final minimal energy structures (Marx *et al.*, 1998b).

2.4. *GC-C Stimulation by Uroguanylin Isomers*

The isomers A and B of uroguanylin-16 and uroguanylin-24 as well as two mixtures of uroguanylin isomers A and B were assessed with respect to their potential to activate GC-C. The relative cellular response caused by synthetic peptides was determined after incubation of human cultured colon carcinoma cells (T84) by a specific cGMP radioimmunoassay (Kaever & Resch, 1985) (Fig. 9).

These results clearly indicate that the A-isomers of uroguanylin-16 and uroguanylin-24 have the potency to activate GC-C with a minimal concentration of between 10^{-7} and 10^{-8} M, similar to guanylin. The amino-terminal extension of eight amino acids contained in uroguanylin-24 had no effect on the cellular cGMP production. In contrast, the isomers B of uroguanylin-16 and -24 had virtually no effect on cGMP level at 10^{-6} M. Two mixtures of uroguanylin isomers A and B in 6:4 and 4:6 ratios were also tested for their ability to generate intracellular cGMP. The amount of cGMP produced by those isomer mixtures was between pure isoform A and B, with a linear relation between the molar ratio of uroguanylin isomers and the detected amount of cGMP produced by T84 cells. Thus, it can be excluded that uroguanylin isoform B acts as an antagonistic ligand of GC-C (Marx *et al.*, 1998b).

2.5. *Structure Comparison with Guanylin and E. coli Enterotoxin*

The two peptides uroguanylin and guanylin show high sequence homology (Fig. 7) and comparable potency to stimulate GC-C (Fig. 11; Klodt *et al.*, 1997; Marx *et al.*, 1998b). Thus they are expected to fold into similar three-dimensional structures. Indeed, the backbone RMSD value for the cysteine rich region between the average structure of uroguanylin-16 isoforms and the structures of guanylin-13 isoforms is 0.14 nm for the A isomers and 0.15 for the B isomers, confirming the similarity between the structures of the corresponding isoforms of uroguanylin and guanylin.

It is generally accepted that *E. coli* heat-stable enterotoxin binds to and activates GC-C with higher efficiency than uroguanylin or guanylin does (Klodt *et al.*, 1997). It also has significant sequence homology to these peptides (Fig. 7). Thus we compared the structures of the uroguanylin isoforms with the crystal structure of *E. coli* heat-stable enterotoxin ST (Ozaki *et al.*, 1991). The backbone RMSD for Cys4 to Cys15 (numbering according to uroguanylin-16) between the average structure of the A-form of uroguanylin-16 and ST is 0.11 nm, indicating that the biologically active A-form of uroguanylin-16 closely resembles the toxic domain of ST (Fig. 10). The corresponding RMSD value for the B-form is 0.45 nm.

The higher activation potency of ST may be due to the third disulfide bond which causes higher rigidity of the three-dimensional structure and thus possibly more effective interaction with the receptor. Furthermore, the additional disulfide bridge may prevent the occurance of a topological stereoisomerism for ST or shift a possible equillibrium between isomers strongly to a structure with A-form like fold.

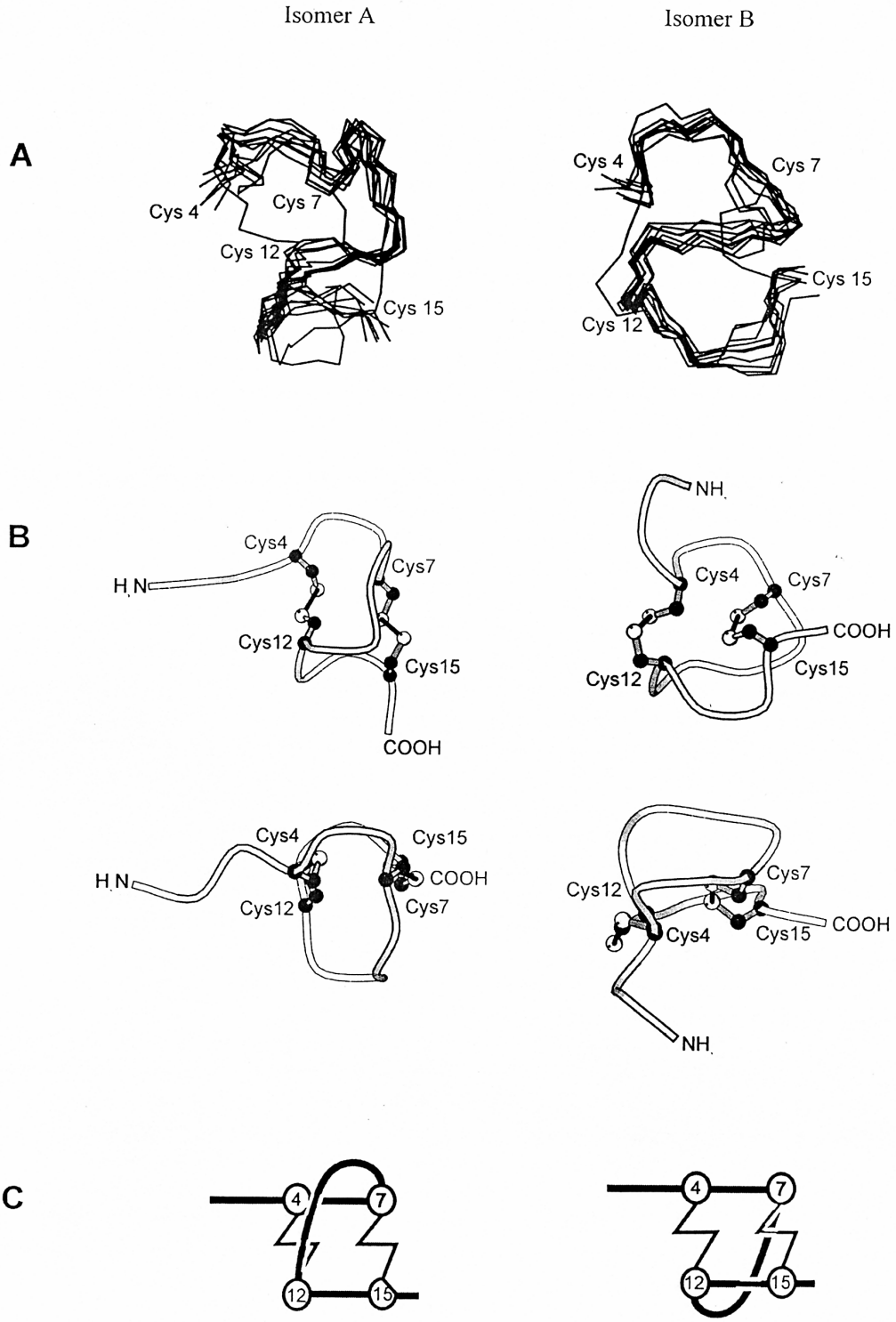

Figure 8. A: Best fit superposition from Cys4 to Cys15 of the backbone atoms of the 10 final structures of each uroguanylin-16 isomer. B: Lowest energy solution structures of uroguanylin-16 isomers. The lower views were obtained from a 90° rotation about a horizontal axis. C: Schematic view of the backbone folds and the disulfide connectivities of uroguanylin-16 isomers. Cysteine residues are represented by encircled numbers.

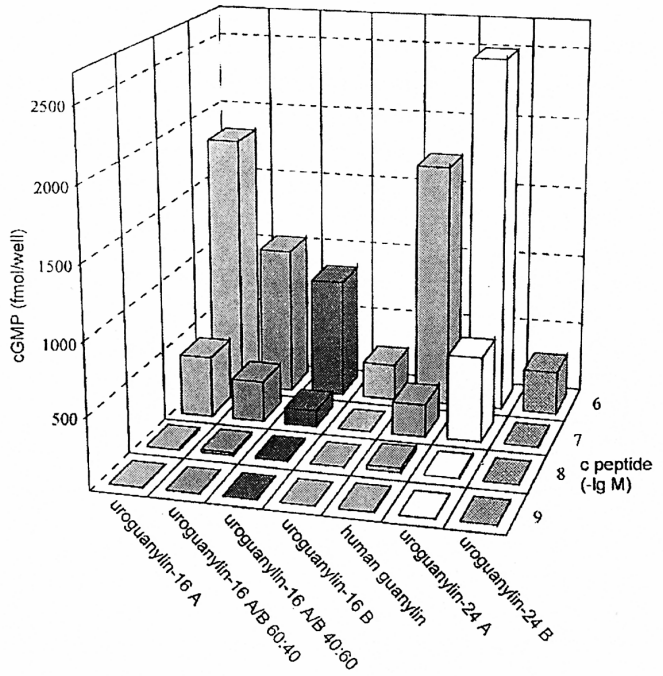

Figure 9. Dose-dependent cGMP accumulation in cultured T84 cells. Intracellular cGMP was measured as a response to the stimulation of guanylate cyclase C by isomers of synthetic uroguanylin-16 and uroguanylin-24 and by mixtures of uroguanylin-16 isomers A and B.

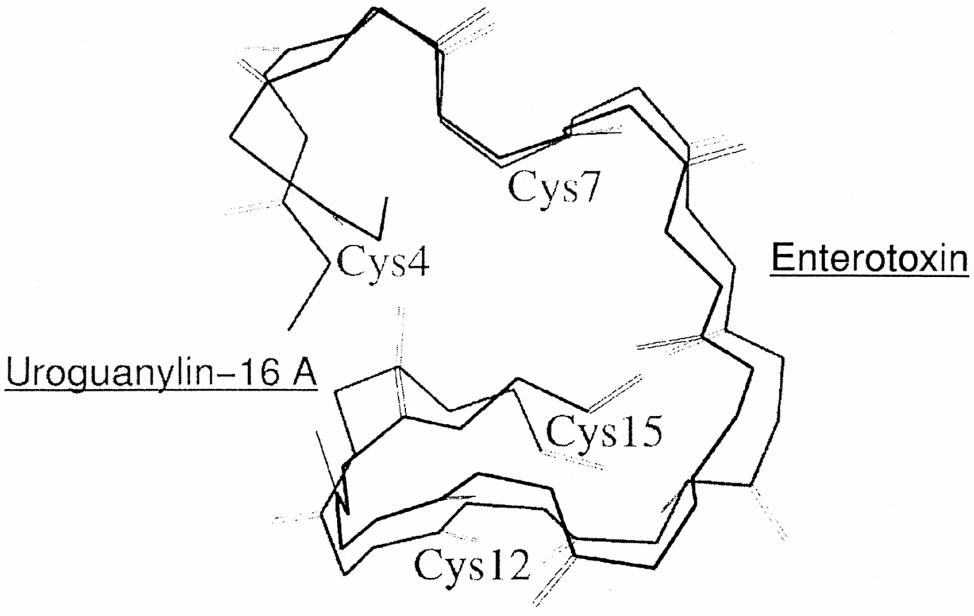

Figure 10. Best fit superposition of Cys4 to Cys15 of uroguanylin-16 A-form with the corresponding region of *E. coli* heat-stable Enterotoxin ST (numbering according to uroguanylin-16).

2.6. Stability and Interconversion of Uroguanylin Isomers

Interconversion kinetics of the separated uroguanylin isomers was studied by HPLC analysis and one-dimensional (1D) NMR spectroscopy. The results show that both isomers pass through a temperature-dependent conversion generating the corresponding stereoisomeric peptide without detectable decomposition or disulfide exchange (Fig. 11).

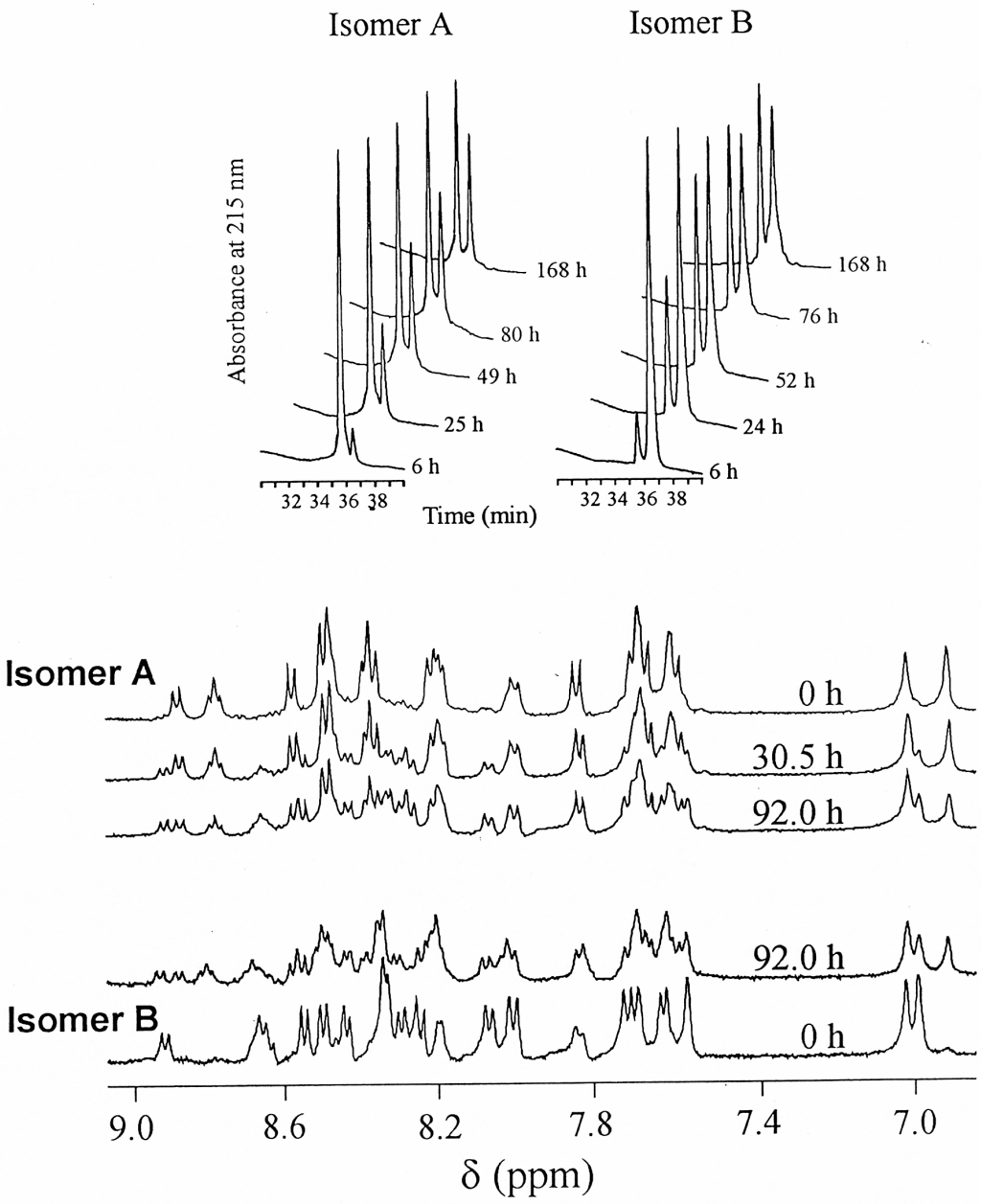

Figure 11. Conversion of uroguanylin isomers. Upper scheme: HPLC analysis of the conversion c uroguanylin-16 isomer A (left) and B (right) at 37°C, pH 4.5. Lower scheme: 1D NMR spectroscopi analysis of the interconversion of uroguanylin-16 isomers. The region of the amide proton resonances shown (400 MHz, 25°C).

1D ^{1}H NMR spectroscopy was used to follow the interconversion of the two isoforms on an atomic level. Measurements of the interconversion of the uroguanylin-16 isomers using 1D-NMR spectroscopy were done at 25 °C over a period of 92 hours. For the initial 24 hours the sample was stored at room temperature, from 24 to 92 hours the sample was incubated at 37 °C between the measurements.

Starting with isomer A the formation of isomer B (and *vice versa*) was followed during the course of 92 hours. New peaks appeared which were unambiguously assigned to B form protons by subsequent 2D NMR spectroscopy. Simultaneously, the intensity of the resonances of the A form protons decreased. After 80 hours an approximately 1:1 mixture of both isoforms was obtained starting with either isomer. The NMR experiments show that no long-lived compound, except the two isoforms, emerges during the interconversion of the uroguanylin isomers (Marx *et al.*, 1998b).

2.7. Mechanism of Isomerisation

Interconversion experiments with isomer concentrations ranging from 0.02 to 5 mM revealed that the isomerization is a concentration-independent process. Furthermore, no indications for an opening and rearrangement of disulfide bonds were found under a variety of conditions. Without breaking of disulfide bridges, there are three different possibilities for the interconversion pathway between the two isoforms (Fig. 12).

The schematic structures of the A- and B-form (Fig. 12) show that an interconversion can be performed by a) pulling the loop between Cys7 and Cys12 through the ring formed by the two disulfide bridges and the loops Cys4 to Cys7 and Cys12 to Cys15, b) pulling the NH_2-terminus through the ring formed by the backbone of residues Cys7 to Cys15 and the disulfide bridge between Cys7 and Cys15, and c) pulling the COOH-terminus through the ring formed by the peptide backbone from Cys4 to Cys12 and the disulfide bridge between Cys4 and Cys12. Pathway a) could be excluded by interconversion experiments using synthetic guanylin derivatives. Neither substitution of the central segment AYA by the more voluminous VNV nor by the sterically smaller AGG sequence influenced the kinetics of interconversion of the two isoforms (Klodt *et al.*, 1997). Also the introduction of bulky diiodo-Tyr9 had virtually no effect on the isomerization kinetics of guanylin (Schulz *et al.*, 1998). b) can be excluded as the interconversion of the uroguanylin-16 isomers and the interconversion of uroguanylin-24, NH_2-terminally extended by 8 amino acids, show kinetically identical characteristics as determined by HPLC analysis. Synthetic derivatives of guanylin and uroguanylin suggest that the isomer conversion follows pathway c): Uroguanylin lacking Leu16 does not form two separable isomers. This peptide shows a guanylin-like chromatographic behavior, that is it shows two inseparable HPLC peaks even at low temperature (Chino *et al.*, 1996). In contrast, synthetic guanylin extended by a carboxy-terminal leucine yields two separable isomers whose stability resembles those of uroguanylin isomers. This effect was intensified by an Lys-Lys extension of the COOH-terminus (Schulz *et al.*, 1998). Thus the velocity of the conformational exchange is under the steric control of the COOH-terminal residue.

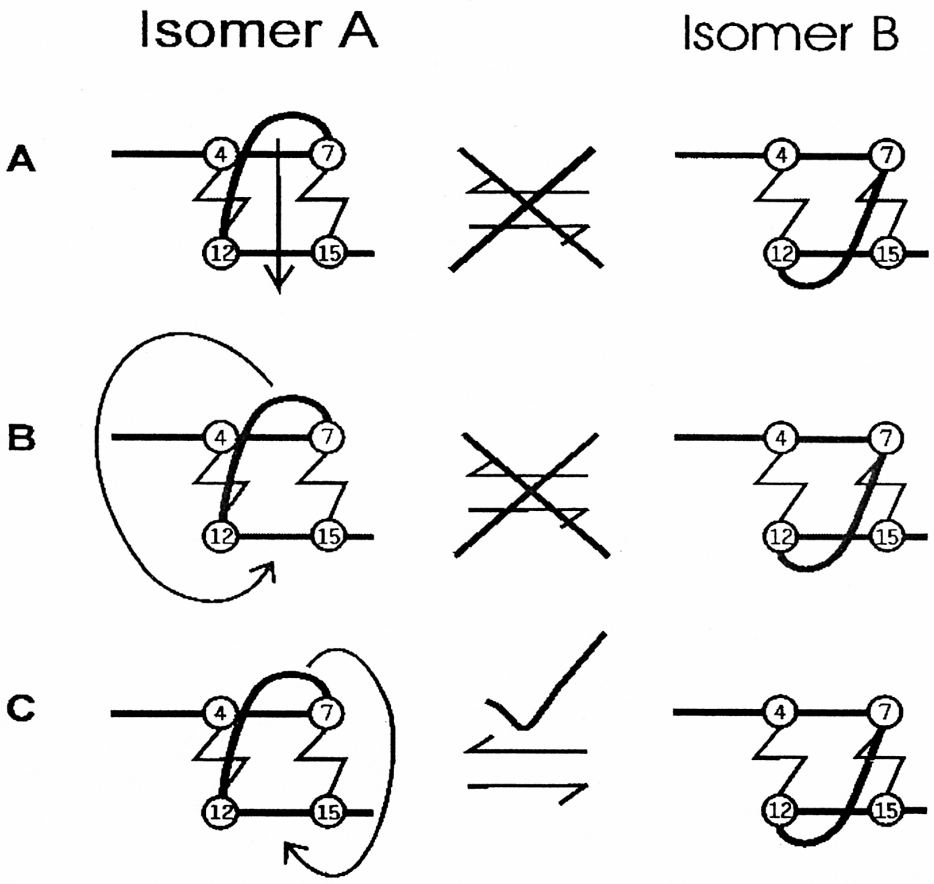

Figure 12. Hypothetic sterical mechanisms of the isomerization without opening and rearrangement of disulfide bonds, suggesting that the isomerization occurs by an intramolecular conformational exchange.

3. CONCLUSIONS

The fact that uroguanylin and guanylin undergo isomerization between two defined topological states distinguishes these peptides from all other known peptide hormones. A fundamental difference between uroguanylin and guanylin is the time constant of interconversion between the respective isomers. The conversion between the uroguanylin isomers follows a significantly slower kinetics and is substantially hindered by the carboxy-terminal leucine. Therefore, the isomers of human uroguanylin may exist physiologically in a non-equimolar ratio. From this study, the isomer bioactive in the stimulation of GC-C could be unambiguously assigned to isomer A, which closely resembles the three-dimensional structure of *E. coli* heat-stable enterotoxin. Although the topological stereoisomerism and the interconversion capacity of uroguanylin isomer B renders it suitable as a storage form of isomer A, a distinct functional role of the B-isomer cannot be excluded

REFERENCES

Brünger, A. T. (1993) X-PLOR version 3.1., Howard Hughes Medical Institute & Yale University, New Haven, CT.

Carpick, B. W. & Gariepy, J. (1993) *Infect. Immun. 61*, 4710-4715.

Caulfield, P. M., McKee, R. L., Goldmann, M. E., Duong, L. T. Fisher, J. E., Gay, C. T., DeHaven, P. A., Levy, J. J., Roubini, E. Nutt, R. F., Chorev, M. & Rosenblatt, M., (1990) *Endocrinology 127*, 83-87.

Chino, N., Kubo, S., Miyazato, M., Nakazato, M., Kangawa, K. & Sakakibara, S. (1996) *Lett. Peptide Sci., 3*, 45-52.

Chorev M. & Rosenblatt, M. (1994) in *The Parathyroids* (Bilezikian J. P., Levine, M. A. & Marcus, R., eds.) Raven Press, New York, pp. 139-156.

Coleman, D. T., Fitzpatrick A., & J. P. Bilezikian (1994) in *The Parathyroids* (Bilezikian J. P., Levine, M. A. & Marcus, R., eds.) Raven Press, New York, pp. 239-258.

Fairman, R., Shoemaker, K. R., York, E. J., Stewart, J. M. & Baldwin, R. L. (1989) *Proteins: Struct. Funct. Genet. 5*,1-7.

Forte, L. R & Currie, M. G. (1995) FASEB J. *9*, 643-650.

Gariepy, J., Judd, A. K. & Schoolnik, G. K. (1987) *Proc. Natl. Acad. Sci. USA 84*, 8907-8911.

Hock, D., Mägerlein, M., Heine, G., Ochlich, P. P. & Forssmann, W.-G. (1997*) FEBS Lett. 400*, 221-225.

Kaever, V. & Resch, K. (1985) *Biochim. Biophys. Acta 1253*, 146-149.

Klodt, J., Kuhn, M., Marx, U. C., Martin, S., Rösch, P., Forssmann, W. G. & Adermann, K. (1997) *J. Pept. Res. 50*, 222-230.

Lopez-Hilker, S., Martin, K. J., Sugimoto, T., and Slatopolsky, E. (1992*) J. Lab. Clin. Med. 119*, 738-743

Marx, U. C., Austermann, S., Bayer, P., Adermann, K., Ejchart, A., Sticht, H., Walter, S., Schmid, F.-X., Jaenicke, R., Forssmann, W.-G. & Rösch, P. (1995*) J. Biol. Chem. 270*, 15194-15202.

Marx, U. C., Adermann, K., Bayer, P., Meyer, M., Forssmann, W.-G. & Rösch, P. (1998a) *J. Biol. Chem. 273*, 4308-4316.

Marx, U. C., Klodt, J.,Meyer, M., Gerlach, H., Rösch, P., Forssmann, W.-G. & Adermann, K. (1998b) *J. Peptide Res. 52,* 229-240.

Ozaki, H., Sato, T., Kubota, H., Hata, Y., Katsube, Y. & Shimonishi,Y. (1991*) J. Biol. Chem. 266*, 5934-5941.

Parsons, J. A., Reit, B. & Robinson, C. J. (1973) *Endocrinology 92*, 454-462.

Segre, G. V., Rosenblatt, M., Reiner, B. L., Mahaffey, J. E. & Potts, J. T. (1979*) J. Biol. Chem. 254*, 6980-6986.

Schulz, A., Escher, S., Marx, U.C., Meyer, M., Rösch, P., Forssmann, W.G. & Adermann, K. (1998*) J. Peptide Res. 52*, 518-525.

Skelton, N. J., Garcia, K. C., Goeddel, D. V., Quan, C. & Burnier, J. P. (1994) *Biochemistry 33*, 13581-13592.

Wishart, D. S., Sykes, B. D. & Richards, F. M. (1992) *Biochemistry 31*, 1647-1651.

Wishart, D. S., Bigam, C. G., Holm, A.,Hodges, R. S. & Sykes, B. D. (1995*) J. Biomol. NMR 5*, 67-81.

Wishart, D. S., Sykes, B. D. & Richards, F. M. (1991*) J. Mol. Biol. 222*, 311-333.